

First constraints on the intrinsic CMB dipole and our velocity with Doppler and aberration

Pedro da Silveira Ferreira,¹ Miguel Quartin^{1,2}

¹*Observatório do Valongo, Universidade Federal do Rio de Janeiro, 20080-090, Rio de Janeiro, RJ, Brazil*

²*Instituto de Física, Universidade Federal do Rio de Janeiro, 21941-972, Rio de Janeiro, RJ, Brazil*

27 April 2022

ABSTRACT

The CMB dipole is usually assumed to be completely due to the relative velocity between the solar system and the CMB restframe. We test this hypothesis by measuring independently the Doppler and aberration effects on the CMB using Planck 2018 data. We remove the contributions arising solely from the conversion of intensity into temperature and arrive at measurements which are independent from the CMB dipole itself. Doppler and aberration are measured independently in the TT and EE maps for both SMICA and NILC. Combining these new measurements with the dipole one we get the first constraints on the intrinsic CMB dipole. Neglecting a dipolar lensing contribution we can put an upper limit on its amplitude: 3.5mK (95% CI). We also obtain the estimate of the peculiar velocity of the solar system which does not assume a negligible intrinsic dipole contribution: $v = (300 \pm 99)$ km/s with $(l, b) = (276 \pm 32, 51 \pm 19)^\circ$ [SMICA] and $v = (300 \pm 100)$ km/s with $(l, b) = (280 \pm 32, 50 \pm 20)^\circ$ [NILC] with negligible systematic contributions. These values are consistent with the peculiar velocity hypothesis of the dipole.

Key words: cosmology: observations, cosmic background radiation, inflation

1 INTRODUCTION

The Cosmic Microwave Background (CMB) temperature dipole is the largest CMB anisotropy not coming from foregrounds, and has been precisely measured since a few decades ago. After removal of the orbital contribution due to the motion of the instrument with respect to the Sun, we are left with the so-called solar dipole, with an amplitude of 3.36208 ± 0.00099 mK (Planck Collaboration I 2020), which is ~ 100 larger than the other multipoles. It is thus fully credited to the proper motion between the solar system and the CMB restframe. If one assumes that the whole dipole has such an origin, one infers a relative velocity of (369.82 ± 0.11) km/s. This velocity estimate is widely reported and regularly used in astronomy in order to convert observed redshifts into heliocentric redshifts.

Nevertheless there exists the possibility that part of the dipolar effect could be due to primordial fluctuations in the last scattering surface. Concrete alternatives to the kinematic scenario were discussed as far back as 30 years ago by Paczynski & Piran (1990), which showed that a large local void could also explain the dipole. This particular scenario was further investigated by e.g. Tomita (2000) and Quartin & Amendola (2010). Turner (1991) proposed a “tilted universe scenario” composed of a superhorizon isocurvature perturbation. An inflationary model which produces similar results was proposed by Langlois (1996). This scenario can be tested by searching for a cosmic bulk flow in the local universe (see e.g. Ma et al. 2011). Complementarily,

the peculiar velocity hypothesis of the dipole can be tested in peculiar velocity surveys, which should converge into the CMB values as the surveyed radius increases. The reported results have nevertheless been inconsistent, as discussed by e.g. Bilicki et al. (2014); Hoffman et al. (2015). Radio galaxies dipole measurements in particular yield results which are a few times higher than what would be expected from the CMB dipole (Colin et al. 2017; Bengaly et al. 2018; Siewert et al. 2020). Another option is to use type Ia supernovae, which can also be used to measure peculiar velocities and bulk flows (Bonvin et al. 2006; Appleby et al. 2015; Huterer et al. 2015; Castro et al. 2016), but the strong inhomogeneity of supernovae data poses a challenge. A more detailed review of cosmic dipole observables is given by Gibelyou & Huterer (2012).

The separation of primordial and kinematic effects in the CMB is not straightforward as in the case of adiabatic perturbations there is a degeneracy between the Doppler effect and the primordial perturbations. As discussed in detail in Roldan et al. (2016), however, this degeneracy can be broken by measuring the Doppler-like and aberration-like couplings in the CMB. In the case of a peculiar velocity these couplings must be present and with well-determined coefficients, as discussed in Amendola et al. (2011) and Notari & Quartin (2012) (see also Yasini & Pierpaoli 2020, for a review). In other scenarios, one of both of these couplings can differ, and therefore by combining the observations of the dipole, Doppler and aberration effects one can independently measure our peculiar velocity and the intrinsic CMB

dipole in a more model-independent way. This is what we pursue in the present work.

The aberration and Doppler couplings of the CMB were shown to be detectable by Planck by [Kosowsky & Kahniashvili \(2011\)](#) and [Amendola et al. \(2011\)](#), and subsequently measured by [Planck Collaboration XXVII \(2014\)](#) following an estimator proposed in [Hanson & Lewis \(2009\)](#). They made use of only the 143GHz and 217GHz channels and measured $v = 384 \text{ km/s} \pm 78 \text{ km/s (statistical)} \pm 115 \text{ km/s (systematic)}$. As explained in that work this measurement however did not distinguish from possible intrinsic contributions and is at least partly degenerate with the standard dipole measurements. In fact, as discussed by [Notari & Quartin \(2016\)](#) similar couplings arise, with higher significance, as a leakage of temperature correlations into thermal Sunyaev-Zeldovich (tSZ) maps, which can be measured by cross-correlating tSZ and TT maps. This cross-correlation was recently detected with significance above 5σ by [Planck Collaboration LVI \(2020\)](#), but this effect is physically *completely* degenerate with the basic dipole measurement and serves only as a cross-check of the model and data.

In this work we improve on the results of [Planck Collaboration XXVII \(2014\)](#) in several ways. First of all, as discussed above we remove the couplings which bring no new information with respect to the dipole. Second, we remove biases in the estimators of aberration and Doppler by simulation the effects using 48^2 combinations of orientations, which ensures no a priori information on the direction of either effect. Third, we rely on the final component separated maps of SMICA and NILC instead on single frequency maps and use the 2018 data release which is more robust than the 2013 one ([Planck Collaboration I 2020](#)). Finally, we make use also of the EE polarization map. These improvements result not only in better precision and much smaller systematic errors, but allow us to both put an upper bound for the first time on the intrinsic CMB dipole and to make an estimate of our peculiar velocity without assuming a negligible intrinsic component.

2 INDEPENDENT ESTIMATORS FOR DOPPLER AND ABERRATION

As discussed in [Challinor & van Leeuwen \(2002\)](#) and [Amendola et al. \(2011\)](#), the primordial temperature $T(\hat{n})$ on the direction \hat{n} seen by an observer with a peculiar velocity β turns into the boosted $T'(\hat{n}')$ following the equation

$$T'(\hat{n}') = \frac{T(\hat{n})}{\gamma(1 - \beta^D \cdot \hat{n}')}, \quad (1)$$

with the aberrated direction \hat{n}' given by

$$\hat{n}' = \frac{\hat{n} \cdot \hat{\beta}^A + \beta^A}{1 + \hat{n} \cdot \hat{\beta}^A} \hat{\beta}^A + \frac{[\hat{n} - (\hat{n} \cdot \hat{\beta}^A)\hat{\beta}^A]}{\gamma(1 + \beta^A \cdot \hat{n})}, \quad (2)$$

where the index A stands for aberration and D for Doppler. In the traditional case where our peculiar velocity is the only source of aberration-like and Doppler-like signals one has $\beta^A = \beta^D = \beta$. In this work instead we separate explicitly the sources of Doppler and aberration in order to further test the peculiar velocity assumption. We will therefore allow also for the case in which $\beta^A \neq \beta^D$. This allows in principle the measurement of a non-adiabatic intrinsic dipole in the

CMB, as discussed in detail in [Roldan et al. \(2016\)](#). Doppler and aberration due to a boost likewise affect the polarization maps and as shown in [Notari & Quartin \(2012\)](#) for Planck there should be non-negligible information in the EE and TE maps.

The above can then be expanded on spherical harmonics. For a given CMB map the coefficients $a_{\ell m}$ can be expanded in a first order approximation in β . For $\beta \sim 10^{-3}$ such an expansion works surprisingly well all the way up to $\ell \sim 3000$ ([Chluba 2011](#); [Notari & Quartin 2012](#)). We therefore proceed this way, which means that Doppler and aberration couple the $\ell, \ell+1$ components but not other $\ell, \ell+n$. We also separate the aberration and Doppler contributions in the final $a_{\ell m}$ s:

$$a'_{\ell m} = a_{\ell m}^{\text{Prim}} + a_{\ell m}^A + a_{\ell m}^D, \quad (3)$$

where $a_{\ell m}^{\text{Prim}}$ are the primordial coefficients. It is convenient to define the quantity

$${}_s G_{\ell m} \equiv \sqrt{\frac{\ell^2 - m^2}{4\ell^2 - 1} \left[1 - \frac{s^2}{\ell^2} \right]}, \quad (4)$$

where $s = 0$ for temperature and $s = 2$ for polarization. We can then write, first considering β only in the z direction

$$a_{\ell m}^A = \beta_z^A (c_{\ell m}^{A,-} a_{\ell-1 m}^{\text{Prim}} + c_{\ell+1 m}^{A,+} a_{\ell+1 m}^{\text{Prim}}), \quad (5)$$

$$a_{\ell m}^D = \beta_z^D (c_{\ell m}^{D,-} a_{\ell-1 m}^{\text{Prim}} + c_{\ell+1 m}^{D,+} a_{\ell+1 m}^{\text{Prim}}), \quad (6)$$

with

$$c_{\ell m}^D = -{}_s G_{\ell m} \quad \text{and} \quad c_{\ell m}^{A,\pm} = (1 \pm \ell) {}_s G_{\ell m}.$$

For the case of only a peculiar velocity ($\beta^A = \beta^D$), following [Amendola et al. \(2011\)](#) one defines the quantity

$$f_{\ell m} \equiv \text{Re} [a_{\ell m}^* a_{\ell+1 m}], \quad (7)$$

and use the following estimator for β

$$\hat{\beta}_z = \left(\sum_{\ell, m} \frac{f_{\ell m}^{\text{obs}} \hat{f}_{\ell m}^{\text{TH}}}{\mathfrak{C}_{\ell} \mathfrak{C}_{\ell+1}} \right) \left(\sum_{\ell, m} \frac{(\hat{f}_{\ell m}^{\text{TH}})^2}{\mathfrak{C}_{\ell} \mathfrak{C}_{\ell+1}} \right)^{-1}. \quad (8)$$

In the above, $\hat{f}_{\ell m}^{\text{TH}}$ is the theoretical expectation divided by β_z (which is independent of β_z at first order)

$$\hat{f}_{\ell m}^{\text{TH}} \equiv \frac{\langle f_{\ell m} \rangle}{\beta_z} = \frac{[c_{\ell+1 m}^{A,+} + c_{\ell+1 m}^D] C_{\ell} + [c_{\ell+1 m}^{A,-} + c_{\ell+1 m}^D] C_{\ell+1}}{\beta_z}, \quad (9)$$

and $\mathfrak{C}_{\ell} \equiv (C_{\ell} + N_{\ell})$ is the sum of the signal and noise spectra.

In the general case where β has all cartesian components, the above is generalized following Appendix B of [Amendola et al. \(2011\)](#). In particular it involves the two point functions $a_{\ell m} a_{\ell+1 m}^{\pm 1}$. One can also make use of the Wigner rotation matrix to rotate (using the $a_{\ell m}$ s) a vector in the z -axis to any other point in the sphere and *vice-versa*.

The above estimator does not consider the important effects of a sky mask. Moreover, it does not account for anisotropic noise and other systematic effects. Applying the mask W and adding noise we get

$$\tilde{a}_{\ell m} = \sum_{\ell' m'} a_{\ell' m'} K_{\ell m \ell' m'} [W] + \sum_{\ell'' m''} a_{\ell'' m''}^{\text{noise}} K_{\ell m \ell'' m''} [W], \quad (10)$$

where $K_{\ell m \ell' m'} [W]$ is the mask kernel and $a_{\ell m}^{\text{noise}}$ the components of the noise map. The new angular spectra for CMB

and noise are

$$\tilde{C}_{\ell_1} = \sum_{\ell_2} M_{\ell_1 \ell_2} C_{\ell_2} \quad \text{and} \quad \tilde{N}_{\ell_1} = \sum_{\ell_2} M_{\ell_1 \ell_2} N_{\ell_2} \quad (11)$$

where a tilde is used when mask and noise are considered. $M_{\ell_1 \ell_2}$ is called the MASTER correlation matrix (Hivon et al. 2002; Pereira et al. 2010).

For $\ell_{\max} \sim 2000$ it is computationally unfeasible to obtain the inverse matrix of $K_{\ell m \ell' m'}[W]$. We instead remove the bias introduced by the mask and noise on the analysis by brute-force through the use of a large number of mock simulations in many sky directions which include both mask and realistic noise simulations. This approach is described in detail in Section 6.

As discussed previously, here we are interested also in the case $\beta^A \neq \beta^D$. This encourages the definition of

$$\hat{f}_{\ell m}^{\text{TH},X} \equiv \frac{c_{\ell+1m}^{X,+} C_{\ell} + c_{\ell+1m}^{X,-} C_{\ell+1}}{\beta_z^X}, \quad (12)$$

for $X = A$ or D and “D,+” = “D,-” = D . However, simply rewriting the estimator above for β^A and β^D separately would not consider the correlations between the aberration and Doppler signals. In fact, since both effects introduce $\ell, \ell + 1$ correlations, they cannot be disentangled exactly. The most precise way to solve this problem would be to minimize a χ^2 numerically for independent β^D and β^A for each vector component:

$$\chi^2(\beta_i^A, \beta_i^D) = 2 \sum_{\ell, m} \frac{[f_{\ell m}^{\text{obs}} - \beta_i^A \hat{f}_{\ell m}^{\text{TH},A} - \beta_i^D \hat{f}_{\ell m}^{\text{TH},D}]^2}{C_{\ell} C_{\ell+1}}. \quad (13)$$

That is nevertheless computationally very demanding considering the number of simulations discussed above to correct the bias of mask and noise. A simpler solution is to just use independent estimators for A and D following Eq. (8) and to remove the correlation *a posteriori* on the data analysis. We adopt a simple, but very effective approach, considering the correlation as a linear effect which is described in detail on Appendix A and which allows an approximately independent measurement of both aberration and Doppler.

We also consider the more traditional case in which one assumes *a priori* that $\beta^A \equiv \beta^D \equiv \beta^B$ as in a standard boost (B) transformation. This corresponds to a boost due to a peculiar velocity in the standard slow-roll inflation scenario, which does not allow for any additional source of Doppler-like and aberration-like couplings. This in general leads to a higher significant detection of these couplings if indeed there are no other sources of such couplings besides a regular boost. On the other hand such a measurement reduces to a simple cross-check, as assuming no other sources of such couplings means that all physical information is already encoded in the high-precision observation of the temperature dipole. The estimated uncertainties in β^A , β^D and β^B of both ideal (without mask and noise) and realistic simulated cases are shown in Appendix B.

3 THE DIPOLE DISTORTION EFFECT ON THE ESTIMATORS

The Planck collaboration does not provide the exact temperature map from their measurements. Instead it converts

intensity maps on different frequencies ν into a temperature map using a linearized relation between both quantities. This procedure introduces distortions in the CMB maps of the order $\sim \beta \delta T / T_0$ which are not due to any primordial process. This was originally pointed out by Kamionkowski & Knox (2003) in the particular case of quadrupole and developed in the general case by Notari & Quartin (2016) (see also Mukherjee et al. 2014). We summarize the main points below.

The default approach since WMAP is to *define* temperature fluctuations ΔT as a linear correction to the intensity fluctuations δI : $\Delta T / T_0(\hat{n}) \equiv \delta I(\nu, \hat{n}) / K(\nu)$, which following Notari & Quartin (2015) we will refer as the *linearized temperature* $L(\hat{n}) \equiv \Delta T / T_0$ – see *ibid.* for the expression $K(\nu)$. If we now extend the expansion to second order we get

$$L(\nu, \hat{n}) = \frac{\Delta T(\hat{n})}{T_0} + \left(\frac{\Delta T(\hat{n})}{T_0} \right)^2 Q(\nu), \quad (14)$$

where

$$Q(\nu) \equiv \frac{\nu}{2\nu_0} \coth \left[\frac{\nu}{2\nu_0} \right]. \quad (15)$$

The second order term shows that higher-order black-body distortions would appear.

Following Notari & Quartin (2016) we expand the linearized temperature L into terms which contain perturbations $\mathcal{O}(10^{-8})$ or higher. These include terms $\mathcal{O}(\beta^2)$ and $\mathcal{O}(\beta \delta T / T_0)$, but not $\mathcal{O}(\beta^3)$ or $\mathcal{O}([\delta T / T_0]^2)$. We also write for the observed dipole $\Delta_{\mathbf{1}} \equiv \beta + \Delta_{\mathbf{1}, \text{int}}$, where $\Delta_{\mathbf{1}, \text{int}}$ is a possible intrinsic dipole in non-standard primordial perturbation scenarios (Roldan et al. 2016). This is the most general way to decompose the terms such as to isolate all effects that carry no new information apart from the dipole, and represents a small extension over the results in Notari & Quartin (2016). We arrive at:

$$\begin{aligned} L(\nu, \hat{n}') = & -\frac{1}{2} \beta^2 + \frac{1}{3} \Delta_{\mathbf{1}}^2 Q(\nu) + \Delta_{\mathbf{1}} \cdot \hat{n}' \\ & + \Delta_{\mathbf{1}}^2 Q(\nu) \left[(\hat{\Delta}_{\mathbf{1}} \cdot \hat{n}')^2 - \frac{1}{3} \right] \\ & + (\beta \cdot \hat{n}') (\Delta_{\mathbf{1}} \cdot \hat{n}') - (\Delta_{\mathbf{1}} \cdot \hat{n}')^2 + \frac{\delta T}{T_0} \\ & + \frac{\delta T}{T_0} [\beta \cdot \hat{n}' + 2 \Delta_{\mathbf{1}} \cdot \hat{n}' (Q(\nu) - 1)] + \mathcal{O}(10^{-9}). \end{aligned} \quad (16)$$

The first two terms are contributions to the monopole, and in particular the second is sometimes called the y -type monopole (Chluba & Sunyaev 2003). The third term is the standard CMB dipole. The next three terms are the Doppler-quadrupole terms. They carry a frequency dependence, originally discussed by Kamionkowski & Knox (2003). Here we expanded the Doppler quadrupole into 3 terms because we allow for an intrinsic dipole; when it is assumed to be zero, only the first term remains. The $\delta T / T_0$ term corresponds to the standard intrinsic CMB perturbations for $\ell \geq 2$. The next terms are the ones we are interested in this paper: they are the Doppler modulation due to a peculiar velocity and the Dipole Distortions (DD), which we discuss below. Note that the aberration effect is contained in \hat{n}' , which is given by Eq. (2).

As discussed in detail by Notari & Quartin (2016), the

crucial point is that the DD does not add any new information not already contained in the very precise measurements of the temperature dipole. Nevertheless, they leave an imprint in the data which is degenerate with the Doppler modulations. Therefore, in order to make measurements of Doppler and aberration which are independent from the basic dipole measurements, one needs to remove this contribution in the analysis. This was first realized by the Planck Collaboration in their measurement of the Doppler modulations (Planck Collaboration XXVII 2014), but they did not attempt to make this separation, and thus their Doppler modulation measurements are driven in part by the dipole itself. We remark that the DD effect is also the source of the couplings in the tSZ maps discussed in the Introduction.

We so far discussed the DD only in terms of the temperature maps, but the same effect is also present in the EE and BB polarization maps (Mukherjee et al. 2014). We therefore also need to remove the DD from the EE map.

In order to remove the redundant DD contribution from our Doppler measurements we need to estimate the effective weight of the frequency dependent contributions arising from $Q(\nu)$ on a given mapmaking procedure. Here we will therefore only consider the Planck mapmaking methods that are mostly based on linear combinations of single-frequency maps on harmonic space which make it possible to calculate the effective DD(ℓ) contribution in a straightforward manner. In particular, from the four main CMB maps we will restrict ourselves to only two: SMICA and NILC. These pipelines rely on the sum of single-frequency maps using weights that varies with ℓ in a way that optimizes the CMB signal extraction.

We can now define the DD factor DD_ℓ^M for each mapmaking method as

$$DD_\ell^M \equiv \sum_\nu 2X_{\ell,\nu}^M [Q(\nu) - 1], \quad (17)$$

where $X_{\ell,\nu}^M$ is the weight of each multipole in the frequency channel ν of map M . The DD generates an effective Doppler-like modulation with an effective velocity $\beta^{\text{DD},M}(\ell) \equiv DD_\ell^M \Delta_1$.

The DD modulation is of the order of $\sim 300 - 600$ km/s, pointing on the dipole direction. Since it is degenerate with any Doppler-like signal, results will be biased towards the dipole direction if this is not removed. We therefore built a pipeline which allows an accurate removal of the DD. Since this is an important issue, we built an alternative pipeline to cross-check the DD removal. Both pipelines are discussed in Section 5. The complete process of reproducing the DD is summarized in Figure 1. In Appendix C we discuss in more detail the DD pipeline.

4 MEASURING THE INTRINSIC DIPOLE

Through a detailed investigation of second-order perturbations on the CMB, Roldan et al. (2016) discussed the effects of different primordial scenarios on the Doppler and aberration signals in the CMB. In particular, assuming a given observed temperature dipole Δ_1 , it was shown that a Gaussian primordial dipolar gravitational potential produces the exact same Doppler couplings in the $a_{\ell m s}$ that a simple peculiar velocity does. This is true irrespective of whether

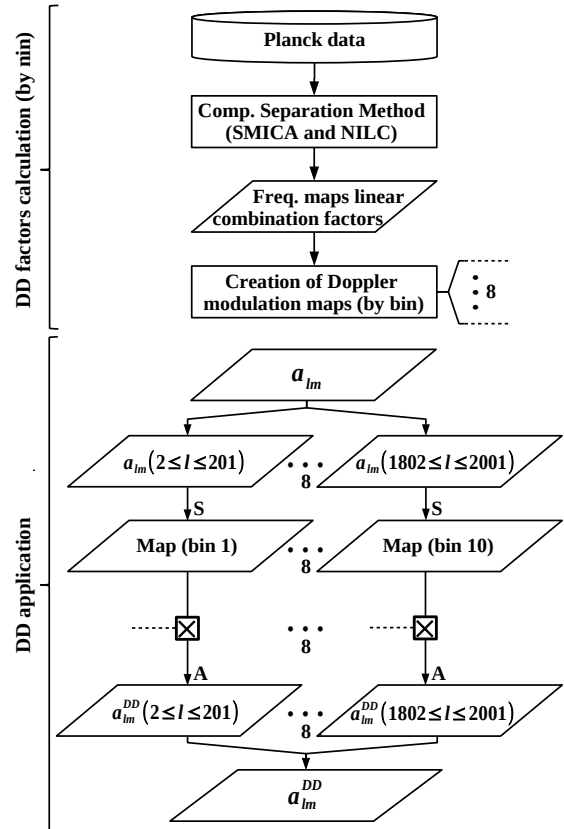


Figure 1. Doppler Distortion pipeline. For each map (I, Q and U) an equivalent Doppler modulation map is created for each multipole bin with the effective Doppler modulation by applying the DD directly on pixel space [see text]. We use 10 bins of $\Delta\ell = 200$. **A** and **S** indicate the use of HEALPix routines *anafast* and *synfast*, respectively.

the perturbation is adiabatic or isocurvature in nature. On the other hand a non-Gaussian dipolar potential produces a different Doppler signature. Moreover, in both cases the aberration signal is different.

This means that a detection of conflicting Doppler, aberration and dipole measurement can hint at the presence of a non-standard large intrinsic dipole. This allows one to test physics beyond the single-field slow-roll inflation model and thus test modifications on recombination physics (see, e.g., Erickcek et al. 2008; Lyth 2013; Dai et al. 2013; Mathews et al. 2015; Meerburg et al. 2017).

We thus separate the temperature dipole into two components: one coming from a Gaussian potential $\Delta_{1,\text{int}}^G$ and another from a non-Gaussian one $\Delta_{1,\text{int}}^{\text{NG}}$, such that the total dipole is the sum of both possibilities

$$\Delta_{1,\text{int}} \equiv \Delta_{1,\text{int}}^{\text{Tot}} \equiv \Delta_{1,\text{int}}^G + \Delta_{1,\text{int}}^{\text{NG}}. \quad (18)$$

The 3 observables are Δ_1 and the aberration and Doppler estimators, β^A and β^D , respectively. Following Roldan et al. (2016) we find that

$$\begin{aligned} \Delta_1 &= \beta + \Delta_{1,\text{int}}^G + \Delta_{1,\text{int}}^{\text{NG}}, \\ \beta^D &= \beta + \Delta_{1,\text{int}}^G + \alpha_1 \Delta_{1,\text{int}}^{\text{NG}}, \\ \beta^A &= \beta + \alpha_2 \Delta_{1,\text{int}}^G + \alpha_3 \Delta_{1,\text{int}}^{\text{NG}}. \end{aligned} \quad (19)$$

The 3 numeric coefficients α_i were shown (ibid.) to be differ-

ent than unity except in some fine-tuned scenarios, and thus the 3 observables above provide independent physical information. In the most general case we have 6 unknowns and 3 observables and the system is not determined. But for any particular intrinsic dipole model these coefficients should be well defined and one can therefore directly measure the intrinsic components of the dipole by measuring aberration and Doppler.

In particular if we for simplicity neglect extra aberration-like couplings (due to dipolar lensing effects) and thus set $\alpha_2, \alpha_3 \ll 1$ we can directly measure the total intrinsic dipole $\Delta_{1,\text{int}}^{\text{Tot}}$. In this case β^A measures directly our peculiar velocity relative to the CMB restframe without the need to assume a negligible $\Delta_{1,\text{int}}$:

$$\Delta_{1,\text{int}}^{\text{Tot}} \simeq \Delta_1 - \beta^A. \quad (20)$$

If we also neglect the Doppler-couplings arising from a non-Gaussian potential (so that $\alpha_1 \ll 1$) we can also conclude that

$$\begin{aligned} \Delta_{1,\text{int}}^{\text{G}} &\simeq \beta^{\text{D}} - \beta^A, \\ \Delta_{1,\text{int}}^{\text{NG}} &\simeq \Delta_1 - \beta^{\text{D}}. \end{aligned} \quad (21)$$

In what follows we will assume for simplicity that all $\alpha_i \ll 1$. On Section 7 we discuss the results found with such analysis. We leave for future work a more complete exploration of different intrinsic dipole scenarios.

5 MASKS AND PIPELINES

As discussed in Section 6 in order to have an accurate estimate we make use of a large number of realistic simulations to fit the effective bias function depending on angular scale. Aiming at robustness, we use two alternative pipelines in order to confirm our results. The Main Pipeline (MP) is the one which we use to quote our final results. The Cross-Check Pipeline (CCP) is an alternative way to remove the DD and which we use to validate our removal method. All steps done to reproduce these simulations are summarized in Figure 2.

To recreate the effects of aberration and Doppler on CMB maps we used the HEALPix-Boost code (Catena & Notari 2013; Catena et al. 2013; Notari et al. 2014),¹ a modified version of HEALPix (Gorski et al. 2005). HEALPix-Boost applies both effects on the mapping between pixel and harmonic space first on the \hat{z} direction and generalises to an arbitrary direction through a Wigner rotation matrix (see, for instance, Amendola et al. 2011) using a modified *alteralm* code.

The pipeline presented in Figure 2 can be summarized as follows. We start with a C_ℓ based on latest Planck 2018 cosmology (Planck Collaboration VI 2020) including lensing. We then produce 3072 Gaussian maps with HEALPix. For each map 3 types of signal are applied using HEALPix-Boost, generating 3 new maps: a complete boost (Aberration + Doppler), a Doppler-only effect and an aberration-only effect. In the most general case, Doppler and aberration may have different orientations, so we simulate each of the 3 effects in 48 different directions (based on the center of

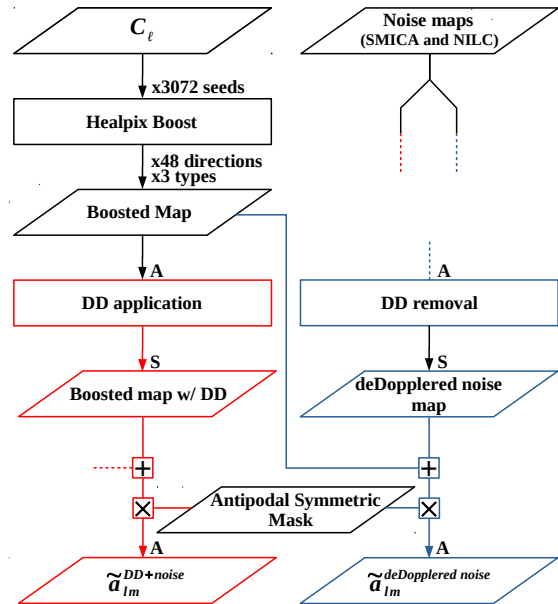


Figure 2. Similar to Figure 1 for the full simulation pipelines MP and CCP. Red (blue) steps are exclusive to the MP (CCP). We generate 64 boosted maps from Planck C_ℓ s for each 48 different directions and apply one of the 3 types of signal: a complete boost (Aberration+Doppler); Doppler only; or aberration only. In total we have 9216 simulations for each SMICA and NILC. The pipelines then diverge. **MP:** The DD is applied in all maps, which are then summed with Planck noise maps and masked. **CCP:** A DD removal (dDD) is applied over the noise maps, which are then summed with the signal (A+D, D or A) and masked.

HEALPix pixels of $N_{\text{side}} = 2$). In each direction and signal type we perform 64 simulations. In all cases we assume $|\beta| = 0.001234$ (i.e. $v \equiv \beta c = 370$ km/s). Note that since all 3 cartesian estimators are independent, this procedure is equivalent to making boosts in each component for different values in the range $[-0.001234, 0.001234]$. We remark that this procedure differs from what was carried out by Planck Collaboration XXVII (2014), where all boosted simulations were on the dipole direction with the dipole amplitude. The motivation behind our procedure is to guarantee that both aberration and Doppler estimators are not biased towards the dipole direction.

After this step there is a divergence between the Main Pipelines (MP) and cross-check pipeline (CCP). The main difference between the MP and CCP is that on MP the DD effect is left to be removed later in the analysis while on the CCP the DD is removed directly on the CMB maps. Since we compute mask and estimator biases directly using simulations each pipeline lead to different biases to be removed on the analysis. The base code to reproduce the MP, including examples, is made available online.²

5.1 MAIN PIPELINE (MP)

For the MP the DD effect is applied over the simulated maps (already with aberration, Doppler or boost signals) and we arrive at $T(\hat{n})^{\text{DD,M}}$ in equation (C7). The maps

¹ www.github.com/mquartin/healpix-boost

² www.github.com/pdsferreira/cmb-aber-dopp

are then summed with the Planck noise maps $N^M(\hat{n})$ for each component separation method M and multiplied by the mask $W(\hat{n})$. In order to avoid any dipolar signature from the mask, which could be a source of bias, we use a mask with antipodal symmetry, as proposed in [Quartin & Notari \(2015\)](#) (see Appendix D). We generate our masks based on the component separation common masks for both temperature (also known as UT78(2018) mask) and polarization (also known as UP78(2018) mask), apodized with a $10'$ Gaussian beam. This process removes an extra 5% of the sky, which diminishes the precision of the estimators by only $\sim 2\%$. Finally we compute the $a_{\ell ms}$ of the final map.

We use these simulations on the statistical and bias analyses. All the steps are carried out using $N_{\text{side}} = 2048$ maps (i.e. ~ 50 megapixels), $\ell_{\text{max}} = 2001$ and considering the realistic beam function given for each of Planck component separation maps.

5.2 CROSS-CHECK PIPELINE (CCP)

As mentioned above in the CCP instead of adding the DD to the simulations, we remove it from the final Planck maps by applying a negative Doppler boost. This DD removal produce “de-Dopplered” (dDD) CMB maps. To be consistent, we also remove the DD from the noise maps, again with a negative Doppler boost. In the CCP, besides the need to adjust the noise maps, the single-frequency weights used in the component separation may no longer be the optimal ones, which is the reason we do not set this as the main pipeline. We nevertheless find that both pipelines give consistent results, which increases the robustness of our findings. The results of the CCP pipeline are presented in Appendix E.

6 BIAS REMOVAL THROUGH BRUTE-FORCE MOCK SIMULATIONS

Besides the DD, other effects need to be accounted for in order to produce unbiased estimations for β^A and β^D . In particular we need to consider the anisotropy of the noise, the effect of masking and the correlation between β^A and β^D . On the MP we minimize the influence of DD, noise and mask by applying a sum and multiplication bias correction on the results of the estimator for each multipole bin of $\Delta\ell = 10$, for each case (aberration, Doppler or boost), cartesian component and mapmaking method.

This bias correction is estimated allowing for a signal on any of 48 sky directions, and any 48^2 combinations of β^A and β^D . The bias is then fitted for each cartesian component estimator separately. As discussed in Section 5, this means that for each component we allow a large range of values of aberration and/or Doppler. The bias correction should thus work for any combination of such components.

In practice, we find the sum and multiplication bias correction factors by minimizing the following χ^2 :

$$\chi^2 = \sum_n \left(\frac{\tilde{\beta}_{nXYi,\text{bin}}^{\text{SIM},M} - \lambda_{Xi,\text{bin}}^M \beta_{nXYi}^{\text{FID}} - \mu_{Xi,\text{bin}}^M}{\tilde{\sigma}_{XYi,\text{bin}}^{\text{SIM},M}} \right)^2, \quad (22)$$

where n is a label for each simulation that identifies the original Gaussian simulation seed and the direction of the (A, D or B) signal, X is the signal applied (A, D or B), Y is the

estimator used (A, D or B), i is the cartesian component and “bin” is one of 200 ℓ -bins between $\ell = 2$ and $\ell = 2001$. SIM means the result of the estimator over a simulation, FID is the fiducial value and M is the mapmaking method (SMICA or NILC). $\lambda_{Xi,\text{bin}}$ is the multiplicative bias and $\mu_{Xi,\text{bin}}$ the sum bias. Our cartesian coordinate system is related to the galactic coordinate system as follows. $\hat{x}: (\ell, b) \rightarrow (0, 0)^\circ$, $\hat{y}: (\ell, b) \rightarrow (90, 0)^\circ$, $\hat{z}: (\ell, b) \rightarrow (0, 90)^\circ$.

The estimated bias must not depend on the signal applied, and only on the estimator used, as we do not know *a priori* the signal. The bias coefficients $\lambda_{Xi,\text{bin}}$ and $\mu_{Xi,\text{bin}}$ therefore cannot depend on β . We use $X = Y$ to fit $\lambda_{Xi,\text{bin}}$ and $\mu_{Xi,\text{bin}}$ and $X \neq Y$ to fit the correlations factors R_i and S_i (see Appendix A). After removing the correlation the results are correct for any combinations of X and Y . The unbiased results with $X = Y$ and $X \neq Y$ are used to calculate the statistical and systematic errors, respectively. The final unbiased results are given by

$$\beta_{nXYi,\text{bin}}^{\text{SIM},M} = \frac{\tilde{\beta}_{nXYi,\text{bin}}^{\text{SIM},M} - \mu_{Xi,\text{bin}}^M}{\lambda_{Xi,\text{bin}}^M}. \quad (23)$$

The bins can be summed to find the vector result

$$\beta_{nXYi}^{\text{SIM},M} = \left[\sum_{\text{bin}=1}^{\text{maxbin}} \frac{\beta_{nXYi,\text{bin}}^{\text{SIM},M}}{\sigma_{nXYi,\text{bin}}^{\text{SIM},M^2}} \right] \left[\sum_{\text{bin}=1}^{\text{maxbin}} \frac{1}{\sigma_{nXYi,\text{bin}}^{\text{SIM},M^2}} \right]^{-1}, \quad (24)$$

so that $\beta_{nXY}^{\text{SIM},M} = \{\beta_{nXYx}^{\text{SIM},M}, \beta_{nXYy}^{\text{SIM},M}, \beta_{nXYz}^{\text{SIM},M}\}$. The value of maxbin depends whether we are using TT or EE. Based on the expected uncertainties shown in Appendix B, we note that there little information in TT (EE) for $\ell > 1800$ ($\ell > 1150$), so we set these value as our maximum multipole in the estimators. We also use $\ell_{\text{min}} = 200$ in both cases as there is very little information on the largest scales.

The estimated cartesian components are our main results. It is useful however to also quote results in galactic spherical coordinates. This however introduce a third bias, as the best fit estimators for each component of a vector does not yield directly the best estimator of its amplitude. In this case we also renormalize the amplitude of the vectors dividing by a factor $\nu_{Xi,\text{bin}}^M$, the “amplitude renormalization”. This ensures that, after correlation removal, $\langle |\beta_{XY}^{\text{SIM},M}| \rangle = |\beta_{XY}^{\text{FID}}|$.

In Figure 3 the residual bias maps are shown. These maps represent the difference between fiducial and recovered results by all estimators, after bias and correlation removal, on simulations for signals applied on different directions. Each arrow starts on the expected direction of the simulated signal and ends on the recovered direction of β , using the average of unbiased results of 64 simulations. The color indicates the $|\beta|$ bias factor. From this figure we can verify that all systematics are under control.

7 RESULTS

The results for the aberration, Doppler and boost estimators, for both SMICA and NILC for the TT, EE and TT+EE cases are shown in galactic coordinates in Table 1. For each entry we show our estimates for the statistical and systematic uncertainties. As discussed the latter are estimated as the residual discrepancy on a given estimator after correcting for the biases due to masking and leakage of signals

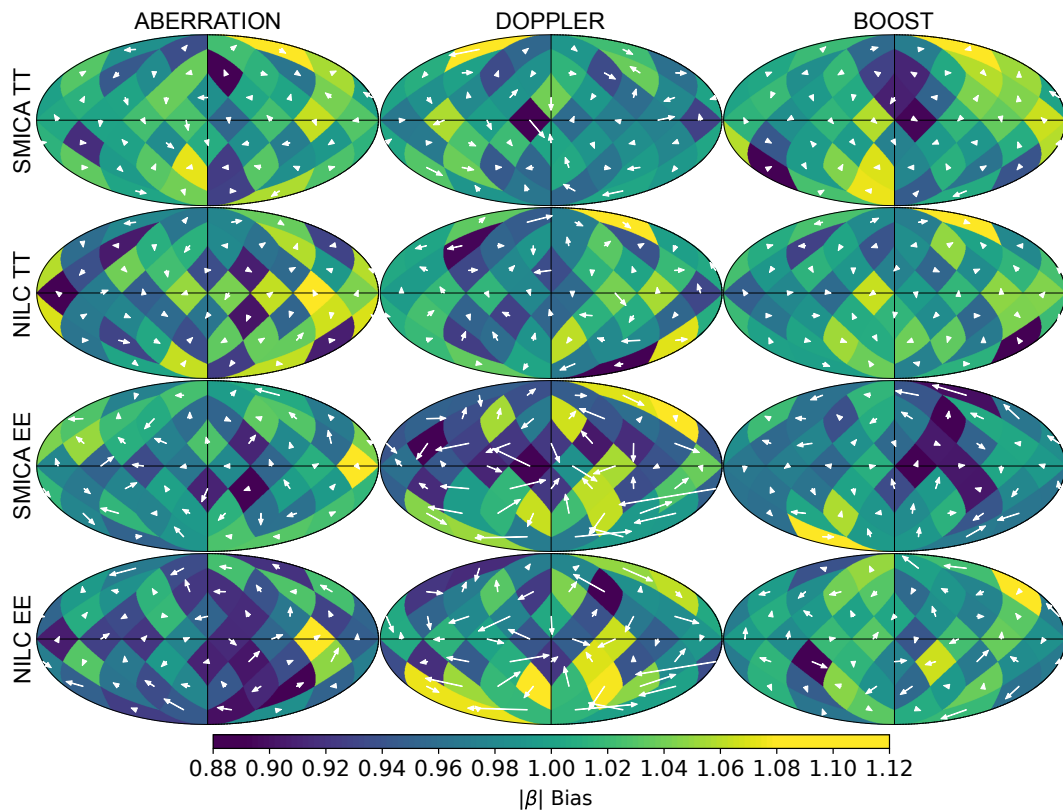


Figure 3. Residual bias maps after bias removal for simulations with noise, mask and the DD effect, for the 3 estimators, component separation method and for TT and EE. White arrows start on the simulated β directions and end on the recovered ones. Color indicates the $|\beta|$ bias factor. Results in each of the 48 directions are the average over 64 simulations with $\ell_{\max} = 1800$ (1150) for TT (EE).

between Doppler and aberration. In all cases except the Doppler amplitude for EE they are negligible.

Figure 4 depicts the confidence intervals for the aberration and Doppler estimators for the TT, EE and TT+EE cases. We show results for different values of ℓ_{\max} up to the maximum values considered here (1800 for TT and 1150 for EE). For aberration we draw the 1 and 2σ (68% and 95.4%) confidence intervals for TT and TT+EE. For EE and for all cases of the Doppler estimator we only draw the 1σ contours as the errors are large and it would otherwise pollute the plots too much. The figures are using the standard Mollweide projection for galactic coordinates. The results for the boost estimator are discussed in Appendix A.

It is clear that the EE channel has in all cases a low signal-to-noise ratio. This was expected *a priori* due to high noise levels in the E-mode $a_{\ell m s}$ (see Appendix B for more details). When combined with TT for the TT+EE results they do lower a bit the statistical errors, and we thus take the TT+EE numbers as our main results.

One can note that the estimators converge smoothly to the final results as ℓ_{\max} increases, and that for TT and TT+EE the Doppler estimator points consistently towards to a region close to the galactic plane. This is incidentally the region that harbors the much-discussed dipolar asymmetry (and the related hemispherical asymmetry). This anomaly, only present at the low multipoles, was originally found in the WMAP results (Eriksen et al. 2004; Hansen et al. 2004; Eriksen et al. 2007; Hoftuft et al. 2009) and has persisted in Planck releases (Planck Collaboration XXIII 2014; Akrami

		TT	$ \mathbf{v} $ [km/s]	$l(^{\circ})$	$b(^{\circ})$
SMICA	Aberration		$360 \pm 130 \pm 13$	$279 \pm 36 \pm 1$	$63 \pm 21 \pm 1$
	Doppler		$410 \pm 150 \pm 13$	$197 \pm 57 \pm 3$	$-7 \pm 33 \pm 1$
	Boost		$330 \pm 100 \pm 11$	$228 \pm 23 \pm .1$	$48 \pm 15 \pm .2$
NILC	Aberration		$330 \pm 130 \pm 13$	$295 \pm 35 \pm 2$	$57 \pm 22 \pm .3$
	Doppler		$340 \pm 150 \pm 10$	$201 \pm 60 \pm 3$	$16 \pm 32 \pm 1$
	Boost		$330 \pm 100 \pm 11$	$242 \pm 22 \pm 1$	$52 \pm 15 \pm .1$
		EE	$ \mathbf{v} $ [km/s]	$l(^{\circ})$	$b(^{\circ})$
SMICA	Aberration		$250 \pm 160 \pm 17$	$272 \pm 66 \pm .1$	$16 \pm 31 \pm 1$
	Doppler		$600 \pm 340 \pm 380$	$275 \pm 103 \pm 6$	$7 \pm 40 \pm 1$
	Boost		$330 \pm 150 \pm 14$	$251 \pm 64 \pm 3$	$24 \pm 31 \pm .5$
NILC	Aberration		$280 \pm 150 \pm 15$	$250 \pm 65 \pm .3$	$30 \pm 31 \pm 1$
	Doppler		$620 \pm 330 \pm 350$	$220 \pm 100 \pm 5$	$7 \pm 41 \pm 1$
	Boost		$360 \pm 150 \pm 15$	$276 \pm 61 \pm 1$	$41 \pm 31 \pm .2$
		TT+EE	$ \mathbf{v} $ [km/s]	$l(^{\circ})$	$b(^{\circ})$
SMICA	Aberration		$300 \pm 99 \pm 13$	$276 \pm 32 \pm .1$	$51 \pm 19 \pm .7$
	Doppler		$390 \pm 140 \pm 13$	$210 \pm 56 \pm 3$	$-2 \pm 30 \pm .5$
	Boost		$321 \pm 84 \pm 9$	$234 \pm 21 \pm .1$	$43 \pm 15 \pm .2$
NILC	Aberration		$300 \pm 100 \pm 10$	$280 \pm 32 \pm .3$	$50 \pm 20 \pm .3$
	Doppler		$380 \pm 140 \pm 10$	$208 \pm 56 \pm 2$	$13 \pm 30 \pm .2$
	Boost		$332 \pm 83 \pm 9$	$250 \pm 22 \pm 1$	$50 \pm 15 \pm .1$

Table 1. Final results in galactic coordinates for each estimator and component separation method (1σ uncertainties). In each case the first error is statistical and the second is the (usually negligible) simulated systematics due to masking, anisotropic noise and leakage between Doppler and aberration. The aberration results are a more model-independent estimate of our peculiar velocity.

		$\beta = \Delta_1$		$\beta = DD = 0$	
		χ^2	σ -value	χ^2	σ -value
SMICA	Aberration	0.8	0.2	18	3.5
	Doppler	5.0	1.4	11	2.4
	Boost	1.4	0.4	45	6.1
NILC	Aberration	0.6	0.1	17	3.4
	Doppler	2.2	0.6	11	2.6
	Boost	0.6	0.3	46	6.2

		$\beta = \Delta_1$		$\beta = DD = 0$	
		χ^2	σ -value	χ^2	σ -value
SMICA	Aberration	0.6	0.1	2.5	0.7
	Doppler	2.2	0.3	3.5	1.0
	Boost	0.6	0.2	2.4	0.7
NILC	Aberration	0.3	0.1	5.3	1.4
	Doppler	1.1	0.3	3.0	0.9
	Boost	0.7	0.2	4.4	1.2

		$\beta = \Delta_1$		$\beta = DD = 0$	
		χ^2	σ -value	χ^2	σ -value
SMICA	Aberration	0.3	0.1	18	3.5
	Doppler	4.6	1.3	12	2.6
	Boost	1.3	0.3	45	6.1
	Aber. & Dopp.	4.9	0.6	30	4.1
NILC	Aberration	0.3	0.1	21	3.9
	Doppler	2.7	0.8	13	2.9
	Boost	0.4	0.1	49	6.4
	Aber. & Dopp.	3.0	0.2	34	4.6

Table 2. Statistical significance for each component separation method and each estimator. The $\beta = \Delta_1$ column assumes the dipole is completely due to a peculiar velocity; the $\beta = DD = 0$ column assumes there is no Doppler or aberration effect of any kind.

et al. 2014). They are usually estimated as a constant several percent modulation for $\ell \leq 70$ or as a modulation with decreasing amplitude with increasing multipole (Hanson & Lewis 2009; Erickcek et al. 2009), and often claimed to be at about the 3σ level. As discussed by Notari et al. (2014), a constant amplitude dipolar modulation is completely degenerate with the Doppler effect, but it is ruled out when considering all scaled observed by Planck (Quartin & Notari 2015). It is therefore interesting to note that our estimator prefers the same region of the sky even though we drop all data with $\ell < 200$. The uncertainties for Doppler are nevertheless large, and there is no statistically significant tension with the dipole direction.

The statistical significance of each estimator result is quoted in two complementary ways. First, we compare each estimator with the standard hypothesis that the dipole is entirely due to peculiar velocity. The second estimate assumes there is no Doppler or aberration effects whatsoever in the data, including the Doppler due to the dipole distortion. The latter allows one to get the overall statistical significance of these $\ell, \ell + 1$ correlations (or signal-to-noise level) in the data. Table 2 summarizes the results in both cases. All results are in agreement with the peculiar velocity hypothesis, and even the Doppler estimators which point to regions close to the galactic plane are in tension with the dipole at less than 1.5σ . Additionally, the full correlations are detected at 3.5 – 3.9σ for aberration, 2.6 – 3.9σ for Doppler, and 6.1 – 6.4σ for boost. For TT+EE we also show the combined significance of Doppler and aberration (4.1 – 4.6σ), which differs

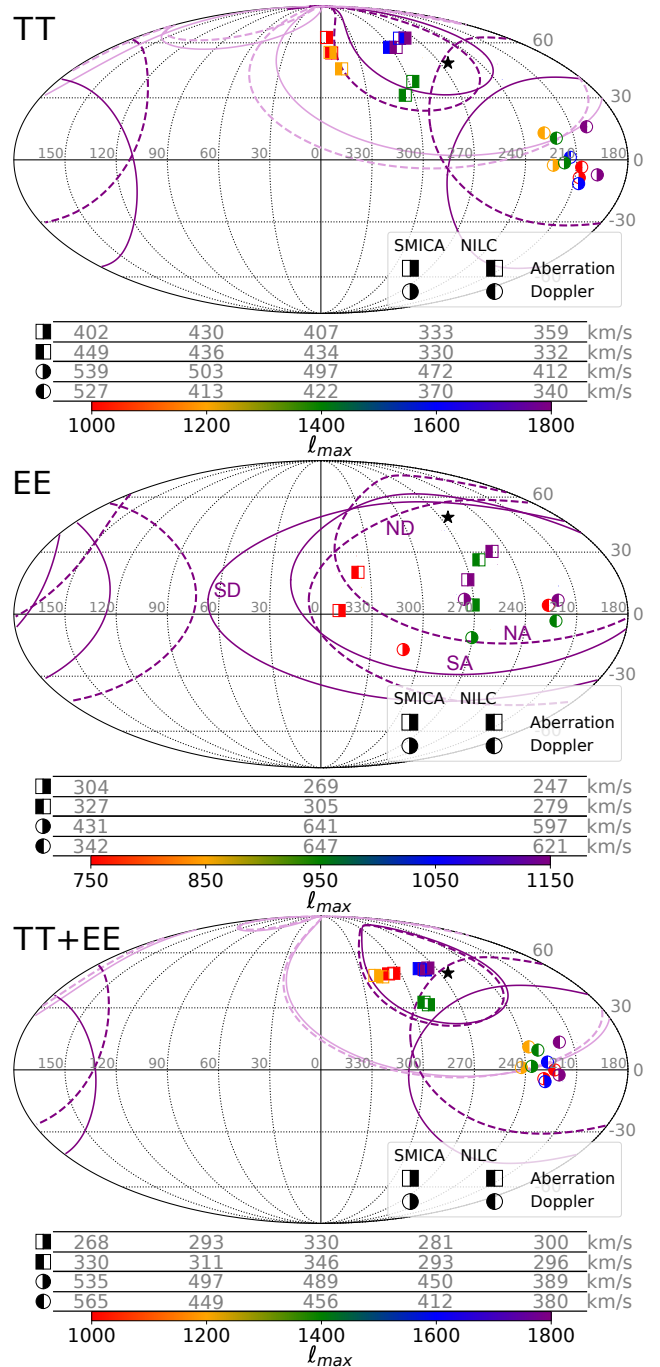


Figure 4. Aberration and Doppler estimations as a function of ℓ_{\max} for the main pipeline for SMICA and NILC. *Top:* TT; *Middle:* EE; *Bottom:* TT+EE. The \star symbol represents the dipole direction. Solid (dashed) contours are the 1 and 2σ (when present) confidence levels for SMICA (NILC). For the EE case and for all the Doppler estimators we only show the 1σ contours as they are already large. For EE we also mark explicitly the Doppler (SD/ND, for SMICA/NILC) and aberration (SA/NA) curves. The values below the Mollweide ellipse represent the amplitude of the estimated vectors.

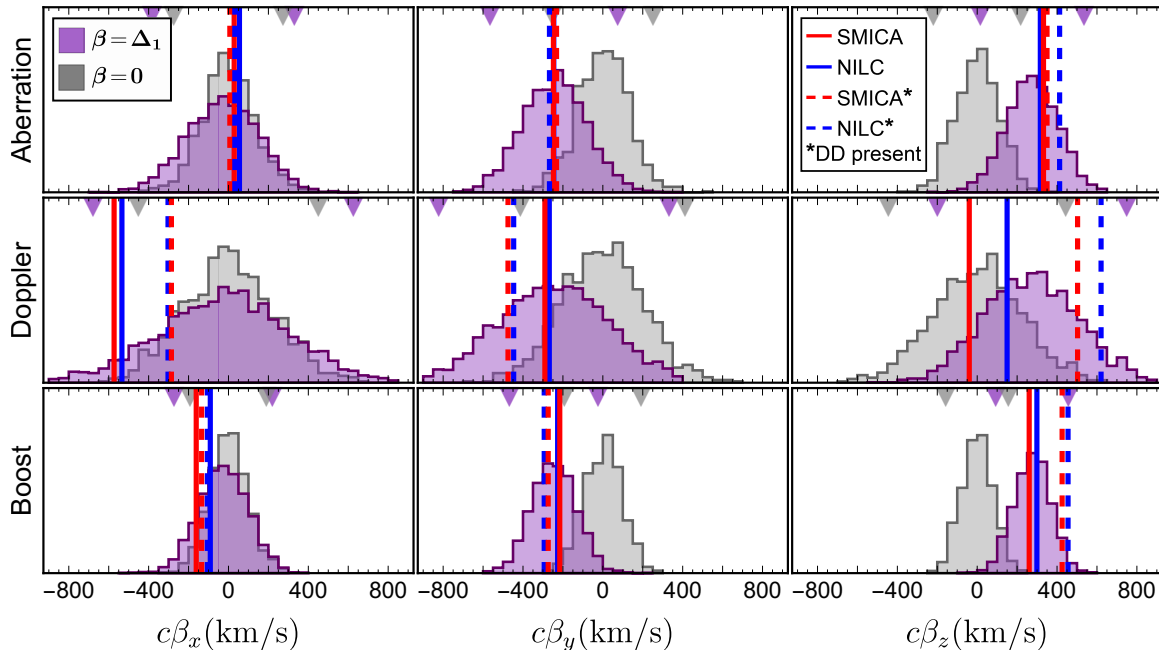


Figure 5. Histograms for $\beta = \Delta_1$ (transparent purple) and $\beta = 0$ (gray) – which is the null hypothesis – using TT+EE, showing the distribution around the expected values. The measurements are shown as vertical lines for SMICA (red) and NILC (blue); in the solid lines we remove the DD effect as it provides no extra information, in the dashed lines it is left included. The ▼ symbols indicates the $\pm 2\sigma$ intervals. Both cases uses $\ell_{\max} = 1800$ and the MP. The solid lines are consistent with the purple diagrams, while the dashed lines and gray histograms yield a large discrepancy. Compare both cases with Table 2.

from the boost estimator in not assuming they point in the same direction. For these estimates we rely on the results for the cartesian components instead of the results for the amplitudes and galactic coordinates, as the former require one less bias term and has uncertainties which are much more Gaussian. The full tables in cartesian coordinates are shown in Appendix F.

The histograms of all our simulations for each cartesian component and each estimator are depicted in Figure 5. These results are the base of Table 2. The purple histograms are the main results, which assume that both Doppler and aberration signals are present (including due to the dipole distortion) and can therefore one leak into the estimator of the other. We also center the histograms in the dipole values, to test the peculiar velocity hypothesis. The gray histograms assume no Doppler or aberration effects are present, which means the leakage is not an issue and therefore the statistical errors are smaller. These are just used to compute the overall significance of the Doppler and aberration in the data, and are centered on zero by definition.

As discussed in Section 4, by measuring Doppler and aberration separately we can constrain two different primordial (intrinsic) origins for the dipole: a Gaussian dipolar potential ($\Delta_{1,\text{int}}^{\text{G}}$, which could be either adiabatic or isocurvature) and a non-Gaussian dipolar potential $\Delta_{1,\text{int}}^{\text{NG}}$. Here we assume for simplicity that the dipolar lensing effect is negligible and that there is no Doppler couplings arising from $\Delta_{1,\text{int}}^{\text{NG}}$. The uncertainty in $\Delta_{1,\text{int}}^{\text{G}}$ is then roughly the aberration and Doppler errors summed in quadrature, while $\Delta_{1,\text{int}}^{\text{NG}}$ has the same precision as the Doppler measurements (since the dipole is measured with much higher precision). The total intrinsic dipole, which we take as the vector sum

TT+EE		Intrinsic dipole	σ -value	95% max [mK]
SMICA		$\Delta_{1,\text{int}}^{\text{G}}$	1.2	8.0
		$\Delta_{1,\text{int}}^{\text{NG}}$	1.3	7.2
		$\Delta_{1,\text{int}}^{\text{Tot}}$	0.1	3.5
NILC		$\Delta_{1,\text{int}}^{\text{G}}$	0.8	7.6
		$\Delta_{1,\text{int}}^{\text{NG}}$	0.8	6.7
		$\Delta_{1,\text{int}}^{\text{Tot}}$	0.1	3.5

Table 3. Statistical significance and 95% upper bound for the intrinsic temperature dipoles measurements using the full TT+EE results for Doppler and aberration. For comparison, the observed dipole is 3.362 mK.

of both options, has the same precision as aberration, which is higher than the one of Doppler. The results for both cases of intrinsic dipole are shown in Table 3. In all cases the values are consistent with zero, so we only quote the maximum 95% confidence level values. Note that the upper limit for the total intrinsic dipole is only marginally higher than the observed dipole. These results exclude for instance the possibility of a ~ 1000 km/s peculiar velocity which is the raw result in many Cosmic Radio dipole measurements (see e.g. Siewert et al. 2020).

We remark that these are the first direct constraints on the intrinsic CMB dipole, the largest possible mode in the last scattering surface. For instance a non-zero measurement of $\Delta_{1,\text{int}}^{\text{NG}}$ would be inconsistent with the slow-roll inflation scenario. Our results are however fully consistent with the peculiar velocity interpretation, as expected by the standard cosmological model.

8 PERSPECTIVES

In over half a century since the discovery of the CMB we have been able to measure temperature, polarization and lensing fluctuations in a very large range of multipoles. After three generations of satellites which pushed the limits on the small scales probed further and further, we are now finally able to put physical constraints on the largest possible scale, the temperature dipole. Our estimates of our peculiar velocity and of the intrinsic CMB dipole are limited by the precision of the aberration and Doppler estimators in Planck data. Doppler in particular has high uncertainty and after removing the uninformative DD contribution is detected at less than 2σ . Future high-resolution CMB experiments can improve this precision by both probing higher multipoles and by measuring the E modes with higher S/N, as discussed by [Notari & Quartin \(2012\)](#) and [Burigana et al. \(2018\)](#).

For the intrinsic dipole, if it has a similar $\sim 0.03\text{mK}$ amplitude as the higher multipoles, it will remain undetectable with this method in the foreseeable future, but ruling out exotic scenarios with $\sim 1\text{mK}$ intrinsic dipoles should be feasible in the near future. Although such a large intrinsic component would be at strong odds with our standard inflation scenario, there has been numerous claims of large scale anomalies in the CMB data, so it is important to also try to detect the largest possible scale in the CMB.

As for our peculiar velocity relative to the CMB rest-frame, it has general application in astronomy. In particular, it is often used to correct all measured redshifts from the observed values to heliocentric ones. Therefore even a subdominant intrinsic dipole contribution would mean that the true velocity is different and could bias observations. Supernova surveys are in particular sensitive to accurate redshift determinations (see e.g. [Calcino & Davis 2017](#)). Model-independent measurements such as the one from the aberration of the CMB allows for more robust redshift corrections.

Both Doppler and aberration effects should be present in all cosmological observables. The SKA telescope is predicted to measure our velocity in 21 cm maps with 10% precision ([Bengaly et al. 2019](#)). Secular extragalactic parallax measurements using GAIA final release is expected to provide a similar precision ([Paine et al. 2020](#)). These is a similar precision to the ones achievable in future CMB experiments ([Burigana et al. 2018](#)). Other proposed ways to measure the intrinsic CMB dipole includes the spectral distortions of the monopole and quadrupole in future spectrometric CMB instruments ([Yasini & Pierpaoli 2017](#)) and the induced effect on the lensing of the CMB for $\ell \gtrsim 3000$ ([Meerburg et al. 2017](#)). It remains to be seen which observable will perform best in the future.

ACKNOWLEDGEMENTS

We would like to thank Hans Kristian Eriksen, Douglas Scott, Maude Le Jeune, Soumen Basak, Suvodip Mukherjee and Alessio Notari for useful discussions. PSF is supported by the Brazilian research agency CAPES (Coordenação de Aperfeiçoamento de Pessoal de Nível Superior). MQ is supported by the Brazilian research agencies FAPERJ and CNPq (Conselho Nacional de Desenvolvimento Científico e Tecnológico).

REFERENCES

- Akrami Y., Fantaye Y., Shafieloo A., Eriksen H., Hansen F., et al., 2014, *Astrophys.J.*, 784, L42, [1402.0870](#)
- Amendola L., Catena R., Masina I., Notari A., Quartin M., Quercellini C., 2011, *JCAP*, 1107, 027, [1008.1183](#)
- Appleby S., Shafieloo A., Johnson A., 2015, *ApJ*, 801, 76, [1410.5562](#)
- Bengaly C., Maartens R., Santos M., 2018, *JCAP*, 04, 031, [1710.08804](#)
- Bengaly C. A., Siewert T. M., Schwarz D. J., Maartens R., 2019, *MNRAS*, 486, 1350, [1810.04960](#)
- Bilicki M., Jarrett T. H., Peacock J. A., Cluver M. E., Steward L., 2014, *ApJS*, 210, 9, [1311.5246](#)
- Bonvin C., Durrer R., Kunz M., 2006, *Phys. Rev. Lett.*, 96, 191302, [astro-ph/0603240](#)
- Burigana C., et al., 2018, *JCAP*, 04, 021, [1704.05764](#)
- Calcino J., Davis T., 2017, *JCAP*, 01, 038, [1610.07695](#)
- Castro T., Quartin M., Benitez-Herrera S., 2016, *Phys. Dark Univ.*, 13, 66, [1511.08695](#)
- Catena R., Liguori M., Notari A., Renzi A., 2013, *JCAP*, 1309, 036, [1301.3777](#)
- Catena R., Notari A., 2013, *JCAP*, 1304, 028, [1210.2731](#)
- Challinor A., van Leeuwen F., 2002, *Phys. Rev.*, D65, 103001, [astro-ph/0112457](#)
- Chluba J., 2011, *MNRAS*, 415, 3227, [1102.3415](#)
- Chluba J., Sunyaev R., 2003, *A&A*, 424, 389, [astro-ph/0404067](#)
- Colin J., Mohayaee R., Rameez M., Sarkar S., 2017, *MNRAS*, 471, 1045, [1703.09376](#)
- Dai L., Jeong D., Kamionkowski M., Chluba J., 2013, *Phys. Rev. D*, 87, 123005, [1303.6949](#)
- Erickcek A. L., Hirata C. M., Kamionkowski M., 2009, *Phys. Rev. D*, 80, 083507, [0907.0705](#)
- Erickcek A. L., Kamionkowski M., Carroll S. M., 2008, *Phys. Rev. D*, 78, 123520, [0806.0377](#)
- Eriksen H., Hansen F., Banday A., Gorski K., Lilje P., 2004, *Astrophys.J.*, 605, 14, [astro-ph/0307507](#)
- Eriksen H. K., Banday A., Gorski K., Hansen F., Lilje P., 2007, *Astrophys.J.*, 660, L81, [astro-ph/0701089](#)
- Gibelyou C., Huterer D., 2012, *MNRAS*, 427, 1994, [1205.6476](#)
- Gorski K., Hivon E., Banday A., Wandelt B., Hansen F., Reinecke M., Bartelman M., 2005, *ApJ*, 622, 759, [astro-ph/0409513](#)
- Hansen F. K., Cabella P., Marinucci D., Vittorio N., 2004, *Astrophys.J.*, 607, L67, [astro-ph/0402396](#)
- Hanson D., Lewis A., 2009, *Phys. Rev. D*, 80, 063004, [0908.0963](#)
- Hivon E., Gorski K., Netterfield C., Crill B., Prunet S., Hansen F., 2002, *ApJ*, 567, 2, [astro-ph/0105302](#)
- Hoffman Y., Courtois H. M., Tully R. B., 2015, *MNRAS*, 449, 4494, [1503.05422](#)
- Hoftuft J., Eriksen H., Banday A., Gorski K., Hansen F., et al., 2009, *Astrophys.J.*, 699, 985, [0903.1229](#)
- Huterer D., Shafer D. L., Schmidt F., 2015, *JCAP*, 12, 033, [1509.04708](#)
- Kamionkowski M., Knox L., 2003, *Phys.Rev.*, D67, 063001, [astro-ph/0210165](#)
- Kosowsky A., Kahnishvili T., 2011, *Phys. Rev. Lett.*, 106, 191301, [1007.4539](#)
- Langlois D., 1996, *Phys. Rev. D*, 54, 2447, [gr-qc/9606066](#)
- Lyth D. H., 2013, *JCAP*, 08, 007, [1304.1270](#)
- Ma Y.-Z., Gordon C., Feldman H. A., 2011, *Phys. Rev. D*, 83, 103002, [1010.4276](#)
- Mathews G., Lan N., Kajino T., Suh I., 2015, *Phys. Rev. D*, 92, 123514, [1406.3409](#)
- Meerburg P. D., Meyers J., van Engelen A., 2017, *Phys. Rev. D*, 96, 083519, [1704.00718](#)
- Mukherjee S., De A., Souradeep T., 2014, *Phys. Rev. D*, 89, 083005, [1309.3800](#)
- Notari A., Quartin M., 2012, *JCAP*, 1202, 026, [1112.1400](#)

- Notari A., Quartin M., 2015, JCAP, 1506, 047, [1504.02076](#)
 Notari A., Quartin M., 2016, Phys. Rev. D, 94, 043006, [1510.08793](#)
 Notari A., Quartin M., Catena R., 2014, JCAP, 1403, 019, [1304.3506](#)
 Paczynski B., Piran T., 1990, ApJ, 364, 341, [ADS](#)
 Paine J., Darling J., Graziani R., Courtois H. M., 2020, ApJ, 890, 146, [1912.11935](#)
 Pereira T. S., Yoho A., Stuke M., Starkman G. D., 2010, [1009.4937](#)
 Planck Collaboration I 2020, A&A, 641, A1, [1807.06205](#)
 Planck Collaboration IV 2020, A&A, 641, A4, [1807.06208](#)
 Planck Collaboration LVI 2020, [2003.12646](#)
 Planck Collaboration VI 2020, A&A, 641, A6, [1807.06209](#)
 Planck Collaboration XXIII 2014, A&A, 571, A23, [1303.5083](#)
 Planck Collaboration XXVII 2014, A&A, 571, A27, [1303.5087](#)
 Quartin M., Amendola L., 2010, Phys. Rev. D, 81, 043522, [0909.4954](#)
 Quartin M., Notari A., 2015, JCAP, 1501, 008, [1408.5792](#)
 Roldan O., Notari A., Quartin M., 2016, JCAP, 1606, 026, [1603.02664](#)
 Siewert T. M., Schmidt-Rubart M., Schwarz D. J., 2020, [2010.08366](#)
 Tomita K., 2000, ApJ, 529, 26, [astro-ph/9905278](#)
 Turner M. S., 1991, Phys. Rev. D, 44, 3737
 Yasini S., Pierpaoli E., 2017, Phys. Rev. Lett., 119, 221102, [1610.00015](#)
 Yasini S., Pierpaoli E., 2020, MNRAS, 493, 1708, [1910.04315](#)

APPENDIX A: REMOVING CORRELATIONS BETWEEN ABERRATION AND DOPPLER

Since both aberration and Doppler introduce $\ell, \ell + 1$ correlations in harmonic space, their estimators have an inherent correlation. To remove this correlation we define 2 coefficients of signal leakage, dubbed R_i (Doppler to aberration) and S_i (aberration to Doppler), for each cartesian component i . We start by assuming that the correlated results $\beta_{X,i}^{[c]}$ are related to the uncorrelated estimators as:

$$\beta_{A,i} \equiv \beta_{A,i}^{[c]} - R_i \beta_{D,i}, \quad (\text{A1})$$

$$\beta_{D,i} \equiv \beta_{D,i}^{[c]} - S_i \beta_{A,i}. \quad (\text{A2})$$

To fit S_i we minimize the following χ^2 :

$$\chi_S^2 = \sum_n \left(\frac{\beta_{nA D i}^{[c]} - \beta_{nA A i}^{\text{FID}} S_i}{\sigma_{D i}} \right)^2 + \sum_n \left(\frac{\beta_{nB D i}^{[c]} - \beta_{nB B i}^{\text{FID}} (S_i + 1)}{\sigma_{D i}} \right)^2, \quad (\text{A3})$$

where n is the simulation id, the second and third sub-indices are the simulation signal and estimator used and $\sigma_{X i}$ the standard deviation of the estimator. The first sum makes use only of simulations where the expected result is null if there is no correlation ($S_i = 0$). On the second sum, which is for the boost case, the Doppler estimation should recover the correct velocity, and hence the factor $(S_i + 1)$. Equivalently

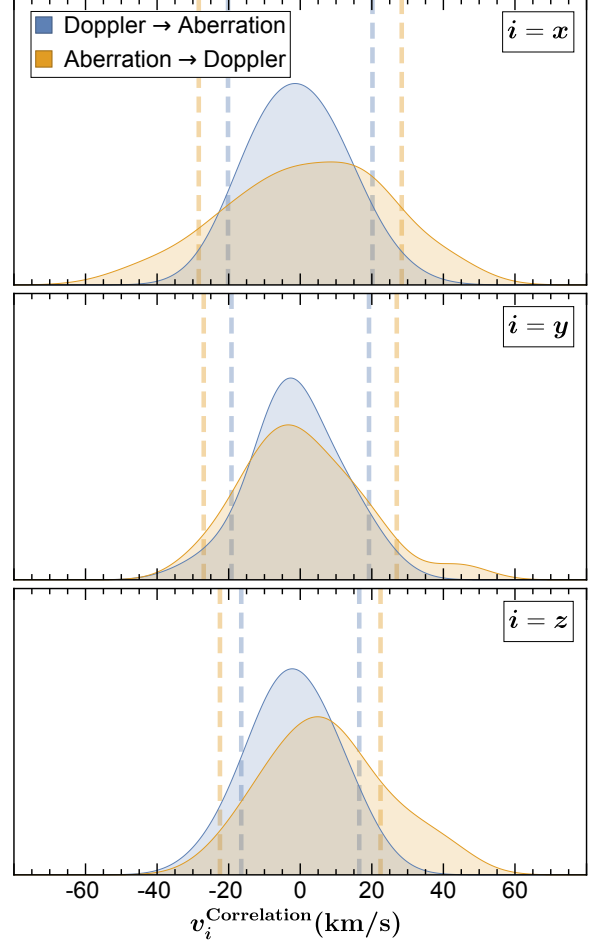


Figure A1. Average residual leakage between the estimators for each cartesian component. Doppler \rightarrow Aberration represents the aberration estimator results for a simulated Doppler modulation of $v_D = 370$ km/s without any aberration, and *vice-versa*. Dashed lines mark the ideal 1σ (standard error) statistical intervals. We conclude that residual leakages are small and can be neglected.

for R_i we have

$$\chi_R^2 = \sum_n \left(\frac{\beta_{nD A i}^{[c]} - \beta_{nD D i}^{\text{FID}} R_i}{\sigma_{A i}} \right)^2 + \sum_n \left(\frac{\beta_{nB A i}^{[c]} - \beta_{nB B i}^{\text{FID}} (R_i + 1)}{\sigma_{A i}} \right)^2. \quad (\text{A4})$$

Using (A1) and (A2) we then get the approximation

$$\beta_{A,i} \simeq \frac{\beta_{A,i}^{[c]} - R_i \beta_{D,i}^{[c]}}{1 - R_i S_i}, \quad \beta_{D,i} \simeq \frac{\beta_{D,i}^{[c]} - S_i \beta_{A,i}^{[c]}}{1 - S_i R_i}. \quad (\text{A5})$$

The effectiveness of this method can be seen comparing the $\beta_{A,i}$ and $\beta_{D,i}$ obtained using this method with the ideal (simulated) case, which we depict in Figure A1. As can be seen the residual leakage are small and can be neglected, and our approach is sufficient for the precision we can achieve.

For the case of a boost (B) we assume a priori that the aberration and Doppler effects are in the same direction, and the correlation between the two estimators are much less important. Moreover, assuming a same direction for both results in greater precision in the estimator. Fig-

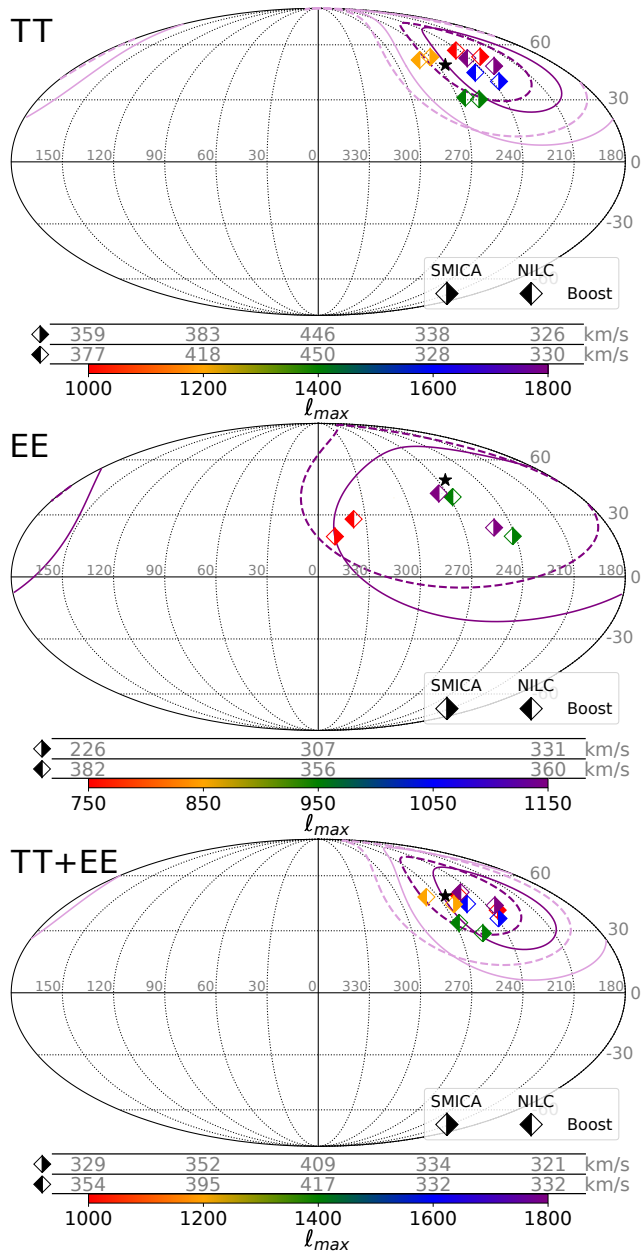


Figure A2. Same as Figure 4 for the boost estimator.

ure A2 shows the B estimator contours, which should be compared with Figure 4. As expected since in this case the aberration and Doppler estimators are constrained to be in the same direction, the uncertainties are smaller. However, the boost estimator is not useful for reconstructing the intrinsic CMB dipole or to get the more model-independent estimates of our peculiar velocity, so its mostly useful as a cross-check.

APPENDIX B: EXPECTED UNCERTAINTIES

Here we compare the expected theoretical uncertainties in each estimator with the simulated uncertainties for both the TT and EE cases. These estimates follow the approach

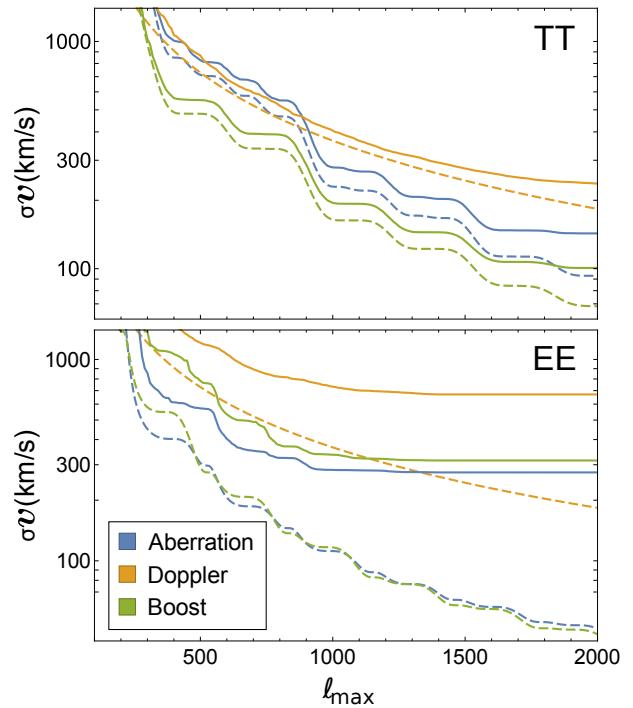


Figure B1. Expected uncertainties in each estimator as a function of l_{\max} . Solid lines represents the measured 1σ errors in our simulations (the average over the 3 cartesian components), dashed lines the ideal theoretical calculations without noise.

in [Amendola et al. \(2011\)](#), but generalized to separate the Doppler, aberration and boost cases. In Figure B1 we depict both the ideal errors without noise and mask, and the total error measured on the MP simulations for the average of the cartesian components estimators as a function of l_{\max} . As can be seen, the EE channel in Planck can provide a $\sim 1\sigma$ measurement of aberration or boost; for Doppler the errors are much larger. This is due to the low S/N in the $a_{\ell m}^E$; with less noise the EE maps could provide a similar precision to TT – see [Notari & Quartin \(2012\)](#) and [Burigana et al. \(2018\)](#). Note also that for EE the partial degeneracy between Doppler and aberration make the boost estimator less precise than the pure aberration one. This result can be proven following the reasoning in Section 5.3 of [Burigana et al. \(2018\)](#).

As discussed in the main text, an unbiased estimate of $|\mathbf{v}|$ require an amplitude normalization factor ν_X^M . This factor ranges from around 1.0 to around 1.8, depending on the estimator (β^A , β^D and β^B), l_{\max} , component separation method (SMICA or NILC) and whether we are using TT or EE.

The cross-correlation maps TE and ET could also be used to provide extra precision. The analysis is however more involved for them: (i) the DD effect is not straightforward; (ii) our simple scheme to remove leakages between signals cannot be used as is; and (iii) our estimators would become correlated (see [Amendola et al. 2011](#)). Finally the expected improvement in precision would be small. We therefore neglect these maps in this present work.

APPENDIX C: PIPELINE FOR REMOVING THE DIPOLE DISTORTION EFFECT

The SMICA's $X_{\ell\nu}^{\text{SMICA}}$ and NILC's $X_{\ell\nu}^{\text{NILC}}$ weights are defined on [Planck Collaboration IV \(2020\)](#)³ as

$$X_{\ell\nu}^{\text{SMICA}} = \frac{W_{\ell\nu}^{\text{Full}}}{b_{\ell\nu}c_\nu} + \mathcal{P}(\ell) \left[\frac{W_{\ell\nu}^{\text{High}}}{b_{\ell\nu}} - \frac{W_{\ell\nu}^{\text{Full}}}{b_{\ell\nu}c_\nu} \right], \quad (\text{C1})$$

$$X_{\ell\nu}^{\text{NILC}} = \frac{\sum_{\text{band}} W_\nu^{\text{NMW,band}} h_\ell^{\text{band}}}{\sum_{\text{band}} h_\ell^{\text{band}}}. \quad (\text{C2})$$

In the above, $\mathcal{P}(\ell)$ is a linear operator that apply a high-pass filter with a multiplicative weight, $W_{\ell\nu}^{\text{Full}}$ and $W_{\ell\nu}^{\text{High}}$ are the weights for each frequency considering all frequencies (Full) or only high frequencies (100, 143, 217, 353, 545 and 857 GHz), $b_{\ell\nu}$ is the beam function and c_ν a calibration factor. $W^{\text{NMW,band}}$ are the mean weights for each single-frequency component for each band, where the needlets h_ℓ^{band} define the extension and weight of the bands. For both SMICA and NILC methods not be biased, for each ℓ , the sum of all single frequency components have to obey

$$\sum_\nu X_{\ell,\nu}^{\text{M}} = 1, \quad (\text{C3})$$

where M stands for the mapmaking method. We can now define the DD factor $\text{DD}_\ell^{\text{M}}$ for each mapmaking method as

$$\text{DD}_\ell^{\text{M}} \equiv \sum_\nu 2X_{\ell,\nu}^{\text{MM}} [Q(\nu) - 1]. \quad (\text{C4})$$

The DD generates an effective Doppler-like modulation with an effective velocity

$$\beta^{\text{DD,M}}(\ell) \equiv \text{DD}_\ell^{\text{M}} \Delta_1. \quad (\text{C5})$$

This spurious effective velocity is depicted in Figure C1 as a function of multipole.

To reproduce the modulation dependence on ℓ we divide the $a_{\ell m}$ into bins, generate the map for each bin separately and apply the modulation on pixel space. We settled on 10 multipole bins of size $\Delta\ell = 200$ ($2 \leq \ell < 2001$) as a good compromise between computational cost and precision: the latter was estimated to be $\sim 1\%$. The DD effect is thus the weighted average

$$\text{DD}_{\text{bin}}^{\text{M}} \equiv \frac{\sum_{\ell=200(\text{bin}-1)+2}^{200\text{bin}+1} (2\ell+1) \text{DD}^{\text{M}}(\ell)}{\sum_{\ell=200(\text{bin}-1)+2}^{200\text{bin}+1} (2\ell+1)}. \quad (\text{C6})$$

We finally define $\beta_{\text{bin}}^{\text{DD,M}} \equiv \text{DD}_{\text{bin}}^{\text{M}} \Delta_1$ and so the transformation on $T(\hat{n})$ is for a given multipole bin is

$$T(\hat{n})_{\text{bin}}^{\text{DD,M}} = \frac{T(\hat{n})_{\text{bin}}^{\text{M}}}{\gamma(1 - \beta_{\text{bin}}^{\text{DD,M}} \cdot \hat{n})}. \quad (\text{C7})$$

Summing the $a_{\ell m}$ s of all 10 binned maps we generate the final map with the complete DD effect, completing the DD pipeline (see Figure 1).

³ Considering deconvolution, calibration and the mask, as per the SMICA propagation code available at https://wiki.cosmos.esa.int/planck-legacy-archive/index.php/SMICA_propagation_code

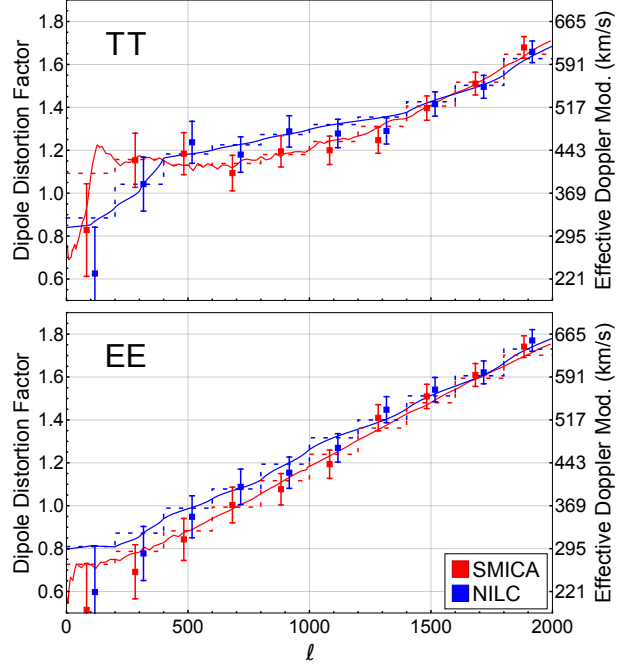


Figure C1. Dipole Distortion values for TT and EE for both SMICA and NILC. Solid lines are the simulated Dipole Doppler factors and dashed stepwise curves are their binned versions. In each bin the estimated average over 1024 simulations and its 1σ uncertainty are also shown. All these results were cross-checked with Planck's dx12 simulations, which yielded equivalent results.

APPENDIX D: THE ANTIPODALLY-SYMMETRIC MASK

As discussed in the main text, for the MP the DD effect is applied over the simulated maps and we arrive at $T(\hat{n})^{\text{DD,M}}$ in equation (C7). The maps are then summed with the Planck noise maps $N^{\text{M}}(\hat{n})$ for each component separation method M and multiplied by the mask $W(\hat{n})$. The final, realistic, map $\tilde{T}(\hat{n})^{\text{DD+noise,M}}$ is

$$\tilde{T}(\hat{n})^{\text{DD+noise,M}} = [T(\hat{n})^{\text{DD,M}} + N^{\text{M}}(\hat{n})] W(\hat{n}). \quad (\text{D1})$$

In order to avoid any dipolar signature from the mask, which could be a source of bias, we use a mask with antipodal symmetry, as proposed in [Quartin & Notari \(2015\)](#). This type of mask has the special property

$$W(l, b) = W(l + \pi, -b), \quad (\text{D2})$$

where (l, b) are the galactic coordinates. So for any masked pixel we mask also the antipodal pixel, ensuring by construction a dipolar symmetry.

Figure D1 depicts both the original and the antipodally symmetric version of Planck UT78(2018) mask, which we employ in this work for the TT maps.

APPENDIX E: RESULTS WITH THE CROSS-CHECK PIPELINE (CCP)

In the CCP instead of adding the DD to the simulations, we remove it from the final Planck maps by applying a negative Doppler boost. To be consistent, we also remove the DD

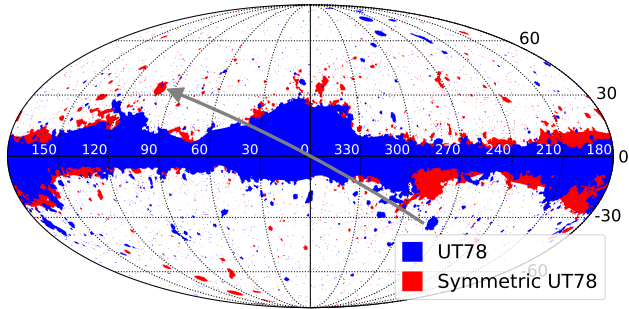


Figure D1. Antipodally symmetric UT78(2018) mask. The grey arrow connects the Large Magellanic Cloud original position and its antipodal position. This removes an extra 5% of sky but helps preventing contamination of the mask in the estimators.

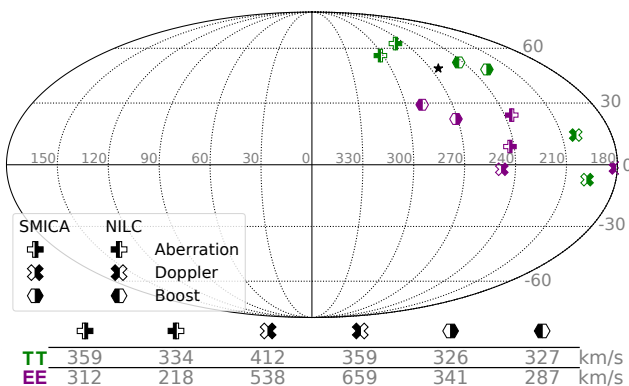


Figure E1. Aberration, Doppler and boost estimations for $\ell_{\max} = 1800$ (1150) for the TT (EE) maps for the cross-check pipeline. The values below the Mollweide plot represent the amplitude of the estimated vectors. The results are similar to the ones in the main pipeline.

from the noise maps, again with a negative Doppler boost. The (ddd) noise maps are calculated in bins, as done in equation (C7):

$$N(\hat{n})_{\text{bin}}^{\text{dDD,M}} = \frac{N(\hat{n})_{\text{bin}}^{\text{dDD,M}}}{\gamma (1 + 2\text{DD}_{\text{bin}}^{\text{M}} \Delta_{\mathbf{1}} \cdot \hat{n})}. \quad (\text{E1})$$

The final noise summed maps are:

$$N(\hat{n})^{\text{dDD,M}} = \sum_{\text{bin}=1}^{10} N(\hat{n})_{\text{bin}}^{\text{dDD,M}}. \quad (\text{E2})$$

$N(\hat{n})^{\text{dDD,M}}$ is then summed with the maps containing the signal (peculiar velocity, Doppler or aberration) and the result multiplied by the mask:

$$\tilde{T}(\hat{n})^{\text{dDD,M}} = [T(\hat{n}) + N(\hat{n})^{\text{dDD noise,M}}] W(\hat{n}). \quad (\text{E3})$$

From this we compute the $a_{\ell m s}$, completing the CCP for simulations.

Figure E1 summarizes our final results using the CCP. A comparison with the results for the main pipeline on Figures 4 and A2 makes it clear that both set of results are in good agreement, which increases the robustness of our main results. It is also clear that both mapmaking techniques

		TT	v_x [km/s]	v_y [km/s]	v_z [km/s]
SMICA	Aberration		30 ± 190	-200 ± 180	390 ± 150
	Doppler		-630 ± 340	-190 ± 300	-80 ± 260
	Boost		-160 ± 130	-180 ± 120	260 ± 100
NILC	Aberration		90 ± 190	-200 ± 180	340 ± 150
	Doppler		-500 ± 340	-190 ± 320	150 ± 260
	Boost		-110 ± 130	-190 ± 120	280 ± 100
		EE	v_x [km/s]	v_y [km/s]	v_z [km/s]
SMICA	Aberration		10 ± 450	-440 ± 350	130 ± 280
	Doppler		110 ± 1200	-1180 ± 920	150 ± 560
	Boost		-170 ± 400	-500 ± 330	230 ± 270
NILC	Aberration		-150 ± 440	-410 ± 320	250 ± 270
	Doppler		-940 ± 1190	-800 ± 830	140 ± 540
	Boost		50 ± 390	-450 ± 310	390 ± 250
		TT+EE	v_x [km/s]	v_y [km/s]	v_z [km/s]
SMICA	Aberration		30 ± 180	-250 ± 160	330 ± 130
	Doppler		-570 ± 330	-290 ± 290	-40 ± 240
	Boost		-160 ± 120	-220 ± 110	260 ± 90
NILC	Aberration		60 ± 170	-250 ± 160	320 ± 130
	Doppler		-530 ± 330	-270 ± 300	150 ± 230
	Boost		-90 ± 120	-230 ± 110	300 ± 90

Table F1. Similar to Table 1 but in cartesian components. Here we only show the total error (statistical + systematics) summed in quadrature, for simplicity.

		Intrinsic dipole	$\Delta_{1,\text{int},x}$ [mK]	$\Delta_{1,\text{int},y}$ [mK]	$\Delta_{1,\text{int},z}$ [mK]
SMICA	$\Delta_{1,\text{int}}^{\text{G}}$		-5.5 ± 3.4	-0.4 ± 3.0	-3.4 ± 2.5
	$\Delta_{1,\text{int}}^{\text{NG}}$		5.0 ± 3.0	0.4 ± 2.6	2.9 ± 2.2
	$\Delta_{1,\text{int}}^{\text{Tot}}$		-0.5 ± 1.6	0.0 ± 1.4	-0.5 ± 1.2
NILC	$\Delta_{1,\text{int}}^{\text{G}}$		-5.4 ± 3.4	-0.2 ± 3.1	-1.5 ± 2.4
	$\Delta_{1,\text{int}}^{\text{NG}}$		4.6 ± 3.0	0.2 ± 2.7	1.2 ± 2.1
	$\Delta_{1,\text{int}}^{\text{Tot}}$		-0.7 ± 1.6	0.0 ± 1.4	-0.4 ± 1.2

Table F2. The measured components of the intrinsic dipole in cartesian components. The error shown is statistical + systematics summed in quadrature.

SMICA and NILC yield consistent results. The largest variation is on the Doppler for the EE map, but this case has a low signal-to-noise ratio, of only around 1/2, so a larger discrepancy was to be expected.

APPENDIX F: RESULTS IN CARTESIAN COMPONENTS

As our main results, the measurements in cartesian coordinates are used to obtain all statistics presented in this work. On Table F1 we show all TT, EE and TT+EE measurements of aberration, Doppler and boost in cartesian coordinates for SMICA and NILC, using $\ell_{\max} = 1800$ for TT and $\ell_{\max} = 1150$ for EE, with TT+EE being the combination of these. Table F2 presents the intrinsic dipole results in cartesian coordinates using TT+EE, considering the definitions on equations (20)–(21). For comparison, $\Delta_{\mathbf{1}}$ in cartesian components is given by $\{-25.6, -244.9, 275.9\}$ km/s.